CARRIER ENVELOPE PHASE STABILIZATION OF A FEMTOSECOND LASER AND IODINE SPECTROSCOPY

A Thesis

by

FENG ZHU

Submitted to the Office of Graduate Studies of
Texas A&M University
in partial fulfillment of the requirements for the degree of

MASTER OF SCIENCE

August 2005

Major Subject: Physics

CARRIER ENVELOPE PHASE STABILIZATION OF A FEMTOSECOND LASER AND IODINE SPECTROSCOPY

A Thesis

by

FENG ZHU

Submitted to the Office of Graduate Studies of
Texas A&M University
in partial fulfillment of the requirements for the degree of

MASTER OF SCIENCE

Approved by:

Chair of Committee,	Hans Schuessler
Committee Members,	George Kattawar
	Lihong Wang
Head of Department,	Edward Fry

August 2005

Major Subject: Physics

ABSTRACT

Carrier Envelope Phase Stabilization of a Femtosecond Laser
and Iodine Spectroscopy. (August 2005)
Feng Zhu, B.S., Tsinghua University, Beijing P.R.China;
M.S., Tsinghua University, Beijing P.R.China
Chair of Advisory Committee: Dr. Hans Schuessler

The carrier envelope (CE) phase of a femtosecond laser was stabilized. The laser produces an ultra stable comb of frequency spanning the visible region and basically is an optical frequency synthesizer and ready for the frequency domain applications.

In this context, the CW stability of the Ti:sapphire laser is discussed to provide a procedure for the femtosecond laser adjustments. In addition, the pulse trains emitted by the femtosecond laser are described analytically to provide a theoretical basis for carrier envelope phase stabilization.

An *f* to *2f* interferometer was used to detect the carrier envelope offset frequency, and a fast photo diode was employed to measure the repetition rate. Two similar designed phase lock loops are used to stabilize both the carrier envelope offset frequency and the repetition rate to the respective reference frequencies. The stability reaches 100mHz for the carrier envelope offset frequency and 10mHz for the repetition rate for a period of up to an hour.

Doppler free iodine saturation spectroscopy was set up to provide a precise frequency reference to which a CW dye laser can be locked on. The near future goal is to accurately measure this frequency stabilized dye laser with the optical frequency synthesizer.

ACKNOWLEDGMENTS

I would like to thank my advisor and committee chair, Dr. Hans Schuessler, for initiating and making it possible to perform this fascinating project. I am very grateful for his guidance throughout all the stages of the research and towards the completion of this thesis. The committee members, Dr. George Kattawar and Dr. Lihong Wang have my thanks for all their time and help.

The Department of Physics, Texas A&M University also has my thanks for the financial assistantship in the past few years. I also acknowledge the Welch foundation for the financial support of this project.

I would also like to express my appreciation to all of the wonderful people who have worked in the femtolab. Dr. Gerhard Paulus, Dr. Alexander Kolomenski, Dr. Xiaojun Liu, Dr. Vladimir Ryjkov, Sergei Jerebtsov, Xudong Xu, Ke Feng, Yunfeng Li, Milan Poudel, Vladimir Lioubimov, it has been a pleasure to work in the laboratory with you.

Prof. T.W. Hänsch and Dr. Thomas Udem from Max Planck Institute(Garching, Germany) have my special thanks for providing the f to $2f$ interferometer. We have a wonderful collaboration. From Dr. Thomas Udem, I have learned a lot, his continued help is crucial to the project. Also many thanks to Dr. Roland Holzwarth, Max Herrmann, Christoph Gohle and Helmut Boückner from Max Planck Institute.

Chris Jaska from Spectra Physics has given me a lot of instructions on the lasers. And I have learned much about lasers from him. For that Chris has my lasting gratefulness.

TABLE OF CONTENTS

CHAPTER Page

LIST OF FIGURES

FIGURE Page

CHAPTER I

INTRODUCTION

With the development of the ultrafast optics, femtosecond laser pulses are generated routinely and applied in many fields. Under the envelope of a femtosecond laser pulse, there is the rapidly oscillating electric field of the carrier wave. For short pulses such as about 50 femtosecond pulse duration or shorter produced by our Ti:sapphire laser, the carrier wave has only about 20 or fewer electric oscillations. In this situation, the phase between the envelope and carrier wave becomes an important factor and should be stabilized. A carrier and envelope phase stabilized laser pulse has many applications both in the time domain and in the frequency domain[1,2].

In the time domain, because the interaction between matter and the intense laser pulse is strongly dependent on the electric field and its location under the intensity envelope of the pulse, the carrier envelope phase is important to extreme nonlinear optics[3]. The carrier envelope phase effect is observed in the situations such as above threshold ionization[4], high-order harmonic generation[5], etc. The ability to control the electric field in a few cycle intense laser pulses means that the interaction between the strong field and the atoms of interest can be studied under repeatable conditions[6].

In the frequency domain, carrier envelope phase stabilization is having a significant impact on optical frequency metrology[7]. The femtosecond pulse has a broad spectrum, and the laser emits a regular train of pulses with a RF repetition rate. This means that the spectrum of the pulse is a frequency comb with many lines under the broad spectrum. If the carrier envelope phase is stabilized, the frequency of each comb line can be determined by two RF frequencies. One is the repetition rate. The other one is called the

---

The journal used for style and format is Physical Review A.

carrier envelope offset frequency. So, by stabilizing the carrier envelope offset frequency and repetition rate, the femtosecond laser can be used as optical frequency synthesizer and can be used to measure essentially any optical frequency[8]. Also, the optical frequency synthesizer provides a reliable way to build optical clocks[9].

The contexts of this thesis are arranged as follow. In Chaper II, I will describe the carrier envelope phase stabilization of a Ti:sapphire femtosecond laser and its applications. Because the performance of our Ti:sapphire femtosecond laser is critical to the carrier envelope phase stabilization, the working principle and basic adjustment of Ti:sapphire femtosecond laser is discussed in Chapter II. An analytic description in both frequency and time domain behavior of the short pulse trains is also included in Chapter II. This gives the theoretical basis for the carrier envelope phase stabilization and the applications.

The f to $2f$ self-referencing technique is used to stabilize the carrier envelope phase. Its optical setup and the phase locked loop will be discussed in Chapter III. In addition, the method used to stabilize the repetition rate is described.

The Doppler free iodine spectroscopy used to lock the dye laser is discussed in Chapter IV. For the frequency domain application of the carrier envelope phase stabilized laser pulses, the scheme of direct frequency measurement of iodine stabilized dye laser frequency is described in Chapter V. This measurement is underway in our laboratory. The summary and an outlook of our future goals is in Chapter VI.

CHAPTER II

TI:SAPPHIRE LASER AND PULSE TRAINS

Ever since their discovery in the 1990's, the Kerr lens mode-locked Ti:sapphire laser has become the dominant choice to generate femtosecond laser pulses. For precision spectroscopy with Ti:sapphire laser, it is critical to stabilize the carrier envelope phase. Also the short pulse trains emitted by the mode-locked Ti:sapphire laser are fundamental to the carrier envelope phase stabilization and its applications.

A. Ti:Sapphire Laser

In 1991, it was observed that when a small perturbation, such as a jerking of the optical table, was carrier out, a CW Ti:sapphire laser went into a pulsed mode[10]. At that time, the method of Kerr lens mode locking was discovered[11]. Because of the excellent performance and simplicity of this method, the Ti:sapphire is now widely used in the femtosecond pulse generation.

The optical setup of a Ti:sapphire laser in our laboratory is show in Fig. 1.

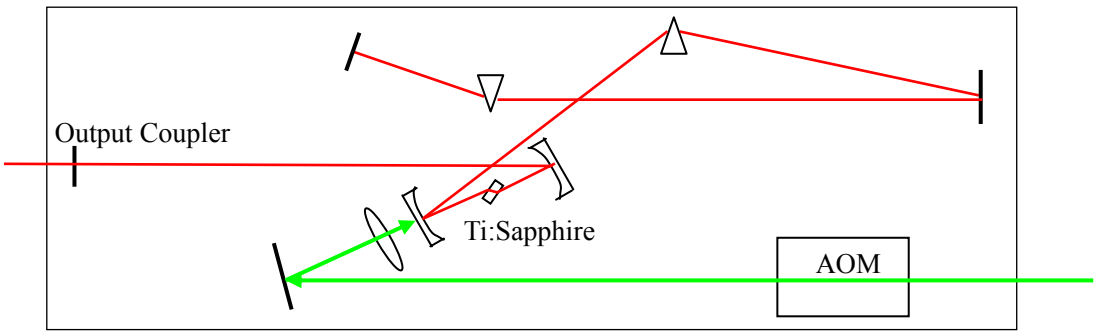

Fig. 1. Ti:sapphire laser

The Ti:Sapphire laser is pumped by a diode-pumped solid state laser(Millennia, Spectraphysics). The Ti:sapphire crystal serves as the gain medium and the nonlinear mode-locking material. A pair of prisms in the cavity compensates the group velocity dispersion in the cavity, mainly caused by the Ti:sapphire crystal.

1. Kerr lens mode-locking

The mode locking mechanism in the Ti:sapphire laser is Kerr lens mode-locking. Due to the optical Kerr effect, the refractive index of a nonlinear material is a function of intensity. Because the beam profile inside the cavity is Gaussian, the Gaussian wave therefore does not have a homogeneous refractive index as it passes through the Ti:sapphire crystal. The refractive index on the axis of the beam is larger than away from the axis. Thus the Ti:sapphire crystal behaves like a converging lens. Hence the beam focuses more with increasing intensity. This is shown schematically in Fig. 2.

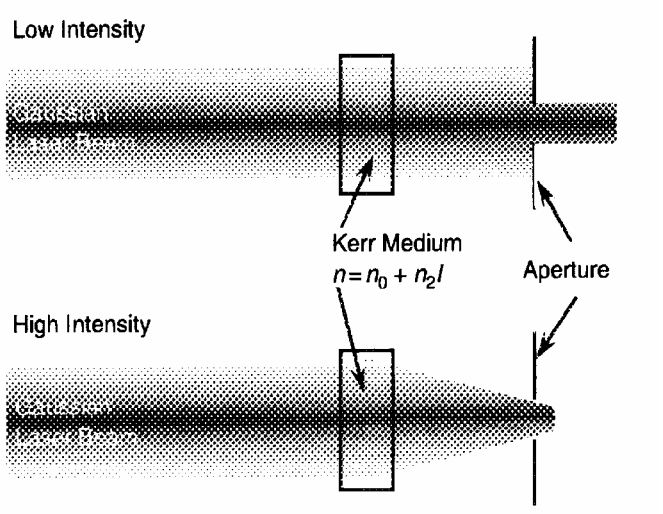

Fig. 2. Kerr lens effect

With a correctly placed effective aperture, the Ti:Sapphire crystal acts like a

saturable absorber. In the crystal, high intensities are focused stronger, and transmit better through the aperture. While the low intensities have losses, the mode-locking pulse regime is more favored over the CW regime. Some Kerr lens mode-locking lasers have an aperture or slit, actually the small size of the gain region can act as one.

2. Stability region

A topic to understand laser operation is to know the stable regime of the Ti:sapphire laser. Since the adjustment of the femtosecond laser is critical in the experiments, it is important to understand the stable diagram and its physical interpretation.

Initially, we consider the CW operation. For the calculation, we can use a schematic diagram of the cavity as shown in Fig. 3. The focal lengths of the curved mirrors are f_1 and f_2, the distance between the end mirror(or output coupler) and the respective curved mirrors are d_1 and d_2 ($d_2 > d_1 > f_1 \approx f_2$). In addition, we label the distance between the curved mirrors is $d_f = f_1 + f_2 + \delta$, δ is the stability parameter.

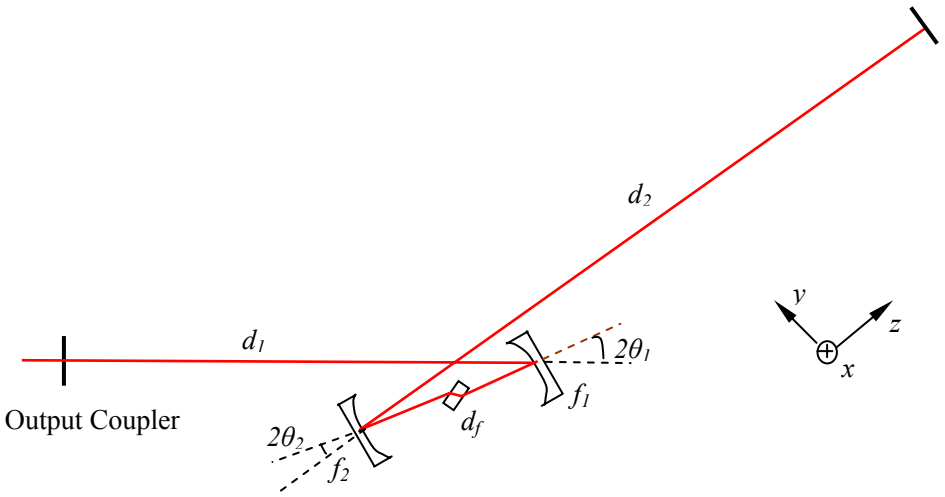

Fig. 3. Cavity diagram

We first make the approximation of a linear cavity without the Ti:sapphire crystal,

and get the transmission matrix of the cavity as follow.

$$T=\begin{pmatrix}1 & d_1\\ 0 & 1\end{pmatrix}\begin{pmatrix}1 & 0\\ -\frac{1}{f_1} & 1\end{pmatrix}\begin{pmatrix}1 & f_1+f_2+\delta\\ 0 & 1\end{pmatrix}\begin{pmatrix}1 & 0\\ -\frac{1}{f_2} & 1\end{pmatrix}\begin{pmatrix}1 & 2d_2\\ 0 & 1\end{pmatrix}*$$
$$*\begin{pmatrix}1 & 0\\ -\frac{1}{f_2} & 1\end{pmatrix}\begin{pmatrix}1 & f_1+f_2+\delta\\ 0 & 1\end{pmatrix}\begin{pmatrix}1 & 0\\ -\frac{1}{f_1} & 1\end{pmatrix}\begin{pmatrix}1 & d_1\\ 0 & 1\end{pmatrix}=\begin{pmatrix}A & B\\ C & D\end{pmatrix}$$

Using the stability condition for a cavity[12],

$$-1\le\frac{A+D}{2}\le 1 \tag{2.1}$$

We can show that when $0\le\delta\le\frac{f_2^{\,2}}{d_2-f_2}$ or $\frac{f_1^{\,2}}{d_1-f_1}\le\delta\le\frac{f_1^{\,2}}{d_1-f_1}+\frac{f_2^{\,2}}{d_2-f_2}$, the cavity is stable. For our laser, the radius of curvature of both curved mirrors is 10cm, thus the focal length of both mirrors is about 5cm. From this it follows that d_1 is about 56cm, and d_2 is about 105cm. So the stability parameter is between [0, 2.5mm] for region I or [4.9mm, 7.4mm] for region II.

3. Astigmatism compensation

Next we consider a folded cavity where astigmatism compensation must be added. For our Ti:sapphire laser, the astigmatism mainly comes from two elements, the curved mirrors and the Brewster angle cut Ti:Sapphire crystal. And we can choose the fold angle so that they can compensate each other[13].

For the curved mirrors, the astigmatism comes from the asymmetry of the oblique incidence. In the sigittal (*xz*) and the tangential(*yz*) plane(as Fig3), according to[14], the Guassian beam is therefore reflected by two different effective focal lengths, related to the normal incidence focal length of the curved mirror $f=\frac{R}{2}$.

$$f_x=\frac{f}{\cos\theta} \tag{2.2}$$

$$f_y = f\cos\theta \tag{2.3}$$

Obviously, considering the stability region, because the actual focal length of the curved mirror is dependent on the incident angle and the *x* or *y* direction, so the stability region on the *x* and *y* direction will be different. Thus the overlap between both regions is then the stability region of the cavity.

Another source of astigmatism is the Brewster angle cut Ti:sapphire crystal. It also acts differently on the *x* and *y* direction as Fig3. It can be evaluated by the effective length l_x and l_y the beams have to travel in the crystal[13].

$$l_x = \frac{t\sqrt{n^2+1}}{n^2} \tag{2.4}$$

$$l_y = \frac{t\sqrt{n^2+1}}{n^4} \tag{2.5}$$

t is the thickness of the Ti:sapphire crystal, and n is the refractive index of it.

Knowing the two astigmatic elements, we compensate the astigmatism of the cavity and aim for maximum overlap of the stability region of *x* and *y* direction. To do this, reconsider the distance d_f between the curved mirror, in the *x* and *y* direction,

$$d_{fx} = f_{1x} + f_{2x} + \delta_x = l_{air} + l_x \tag{2.6}$$

$$d_{fy} = f_{1y} + f_{2y} + \delta_y = l_{air} + l_y \tag{2.7}$$

For the *x* and *y* direction, l_{air} is the same. Thus,

$$\delta_x - \delta_y = l_x - l_y - (f_{1x} - f_{1y}) - (f_{2x} - f_{2y}) = 0 \tag{2.8}$$

With this condition, the stability parameters in *x* and *y* direction are equal, and the astigmatic compensation condition is,

$$\frac{t(n^2-1)\sqrt{n^2+1}}{n^4} = f_1 \sin\theta_1 \tan\theta_1 + f_2 \sin\theta_2 \tan\theta_2 \tag{2.9}$$

For our laser, t is 3.0mm, n is 1.76, f_1=f_2=50mm, then one of the approximate

solutions is 5° for θ_1 and 8° for θ_2. The parameters calculated above are very helpful to the adjustment of the femtosecond laser, even though it's very hard to measure and determine such small angles in the infrared laser beam.

4. Beam radius

For the laser adjustment, we can see the beam profile at mirrors with an infrared viewer. The beam radii at the end mirror and the output coupler can provide good observation parameters. To derive this spot size, let's again consider a linear cavity. In the *x* direction, The radii of curvature of the mirrors and the distance of the equivalent resonator are calculated as shown in Fig. 4:

Fig. 4. Equivalent resonator diagram

For the calculation, we need to compare the *ABCD* transmission matrix for both systems, since they make up the equivalent resonator.

$$\begin{pmatrix} 1 & 0 \\ -\frac{1}{f} & 1 \end{pmatrix}\begin{pmatrix} 1 & 2d \\ 0 & 1 \end{pmatrix}\begin{pmatrix} 1 & 0 \\ -\frac{1}{f} & 1 \end{pmatrix} = \begin{pmatrix} 1 & D \\ 0 & 1 \end{pmatrix}\begin{pmatrix} 1 & 0 \\ -\frac{2}{R} & 1 \end{pmatrix}\begin{pmatrix} 1 & D \\ 0 & 1 \end{pmatrix}$$

Thus $D = \dfrac{df}{f-d}$ $R = -\dfrac{f^2}{d-f}$, so

$$R_{1x} = -\frac{f_{1x}^2}{d_1 - f_{1x}} \tag{2.10}$$

$$R_{2x} = -\frac{f_{2x}^2}{d_2 - f_{2x}} \tag{2.11}$$

And the length of the equivalent resonator is:

$$T_x = D_{1x} + D_{2x} + f_{1x} + f_{2x} + \delta = R_{1x} + R_{2x} + \delta \tag{2.12}$$

For such an equivalent resonator, in x direction the central beam waist ω_0 is then given by[15]:

$$(\frac{\pi\omega_0^2}{\lambda})^2 = \frac{T_x(R_{1x} - T_x)(R_{2x} - T_x)(R_{1x} + R_{2x} - T_x)}{(R_{1x} + R_{2x} - 2T_x)^2} \tag{2.13}$$

The central beam waist ω_0 versus the relative stability parameter $\delta / \delta_{\max}$ can be plotted as Fig. 5. Here the

$$\delta_{\max} = \frac{f_{1x}}{d_1 - f_{1x}} + \frac{f_{2x}}{d_2 - f_{2x}} \tag{2.14}$$

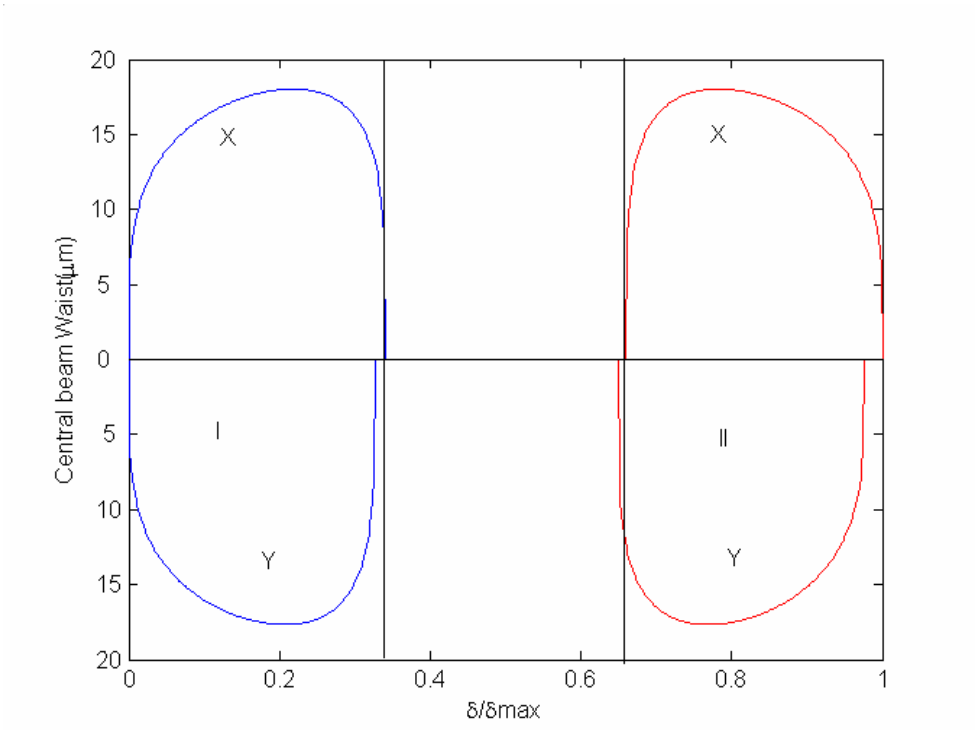

Fig. 5. Central beam waist versus the relative stability parameter

The cavity parameters are: the radius of curvature of both curved mirrors is 10cm, θ_1 is 5°, θ_2 is 8°, d_1 is about 56cm, and d_2 is about 105cm. And for the wavelength λ, we use the 800nm.

In the diagram, the upper part is for the x direction, the lower part is y direction. As can be seen from Fig. 5, the central beam waists in x and y direction overlap quite well for close angles θ_1 and θ_2, thus in this approximate case, the beam profile can be treated as Gaussian in two dimensions.

By using the *ABCD* matrix to trace the Gaussian beam from the central beam waist to the output coupler and end mirror, the beam radius at the output coupler(1) and end mirror(2) can be plotted as shown in Fig. 6.

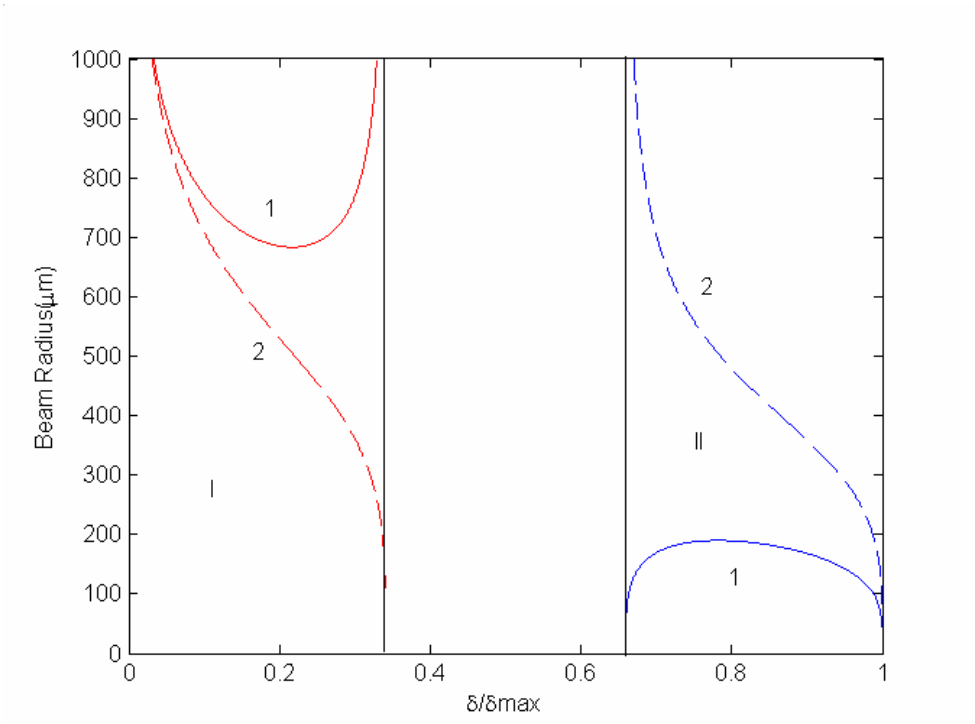

Fig. 6. Beam radius at output coupler[1] and end mirror[2]

The main result is that beam radius at the output coupler is strongly dependent on the position in either stability region. It is recommended Kerr-lens mode locking Ti:sapphire laser should be operated at the upper edge of stability region I[16,17]. This follows from the considerations such as self amplitude modulation introduced by the gain medium, which means a power-dependent change in both the position and diameter of the central beam waist between the focusing mirror if the gain medium is placed in the resonator. Observing the change of beam profile at the output coupler is very helpful to the adjustment of the femtosecond laser.

B. Pulse Trains

1. Time domain and frequency domain description.

In the time domain, when the Kerr lens mode-locking is in effect, the pulse is periodically bouncing back and forth between the end mirror and the output coupler in the cavity with the repetition rate. The carrier wave and envelope travel at different velocities, since the pulse propagates through some dispersive material, such as Ti:sapphire crystal, When the pulse circulates inside the cavity with length L, the pulse envelope $A(t)$ propagates with the group velocity, and the carrier wave inside the envelope propagates with the phase velocity. Each time when the pulse hits the output coupler, part of the pulse will exit from the cavity with a certain carrier envelope phases relative to the initial pulse. As a result, the output pulses are separated by the round trip time T, the carrier wave shifts a phase angle $\Delta\varphi$ with respect to the envelope after each round trip time T. The round trip time T is

$$T = \frac{2L}{v_g} \tag{2.15}$$

The electric field amplitude E of the laser pulses can be written as

$$E(t) = A(t)\exp(-i2\pi f_c t) = \sum_n A_n \exp(-i2\pi(f_c + nf_r)t) \tag{2.16}$$

Where f_c is the carrier frequency, A_n is the Fourier components of *A(t)* and f_r is the repetition rate

$$f_r = \frac{1}{T} = \frac{v_g}{2L} \tag{2.17}$$

For the f_c carrier frequency, we can rewrite it as $f_c = kf_r + f_o$, where *k* is an integer, and f_o is called the carrier envelope offset frequency and usually $f_o < f_r$. Thus *E* can be written as,

$$E(t) = \sum_m A_m \exp(-i2\pi(f_o + mf_r)t)$$

So after a round trip time *T*, it holds

$$E(t+T) = \sum_m A_m \exp(-i2\pi(f_o + mf_r)t \cdot \exp(-i2\pi f_o T) = E(t)\exp(-i2\pi f_o / f_r) \tag{2.18}$$

Thus the carrier envelope phase difference from pulse to pulse is

$$\Delta\varphi = 2\pi \frac{f_o}{f_r} \tag{2.19}$$

And in many round trip procedures, the femtosecond laser emits the same amount of short pulses. The frequency mode is

$$f_m = f_o + mf_r \tag{2.20}$$

where the *m* is a large integer with magnitude around million. Thus in the frequency domain, the frequency spectrum of the infinite pulse trains is a frequency comb of many lines separated by the repetition rate under the broad spectrum of a single pulse, it is shown as Fig. 7.

For a more complicated pulse, such as a chirped pulse, where the frequency varies with time, the carrier wave varies across the pulse. In this case the envelope function *A(t)* becomes complex in value. If the chirp is same from pulse to pulse, the comb structure

still remains[1].

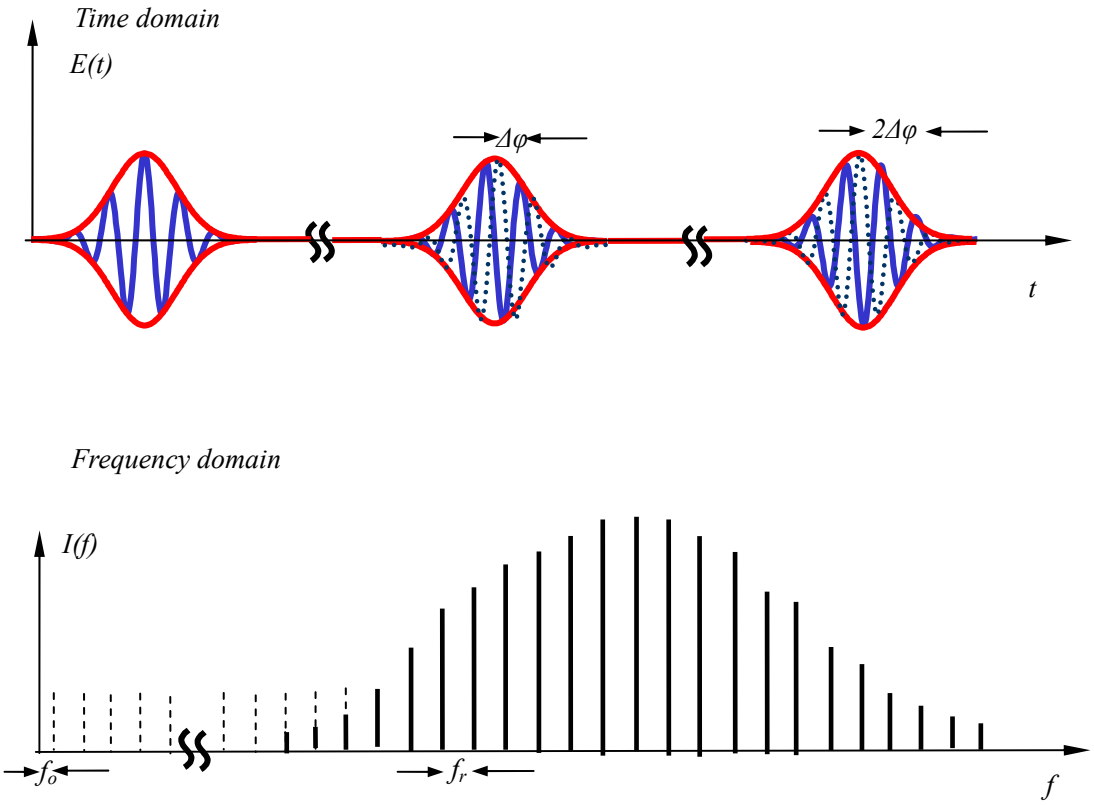

Fig. 7. Description of short pulse trains in time domain and frequency domain

2. Carrier Envelop offset frequency and repetition rate

From Eq.(2.19), it can be seen that the pulse to pulse carrier envelop phase shift is dependent on the carrier envelop offset frequency and the repetition rate. For the carrier envelop phase stabilization, the pulse to pulse phase shift should be stabilized. For many of the time domain applications, it is sufficient to stabilize the ratio of the offset frequency and the repetition rate. For example, if the ratio is 1/4, that means for every pulse the carrier wave evolves π/2 phase angle, thus the every fourth pulse looks the

same. In this way, the same seeded pulses are can be delivered to an amplifier for the further amplification. Amplifiers operate in general at a much lower repetition rate(1-10kHz) than the Ti:sapphire oscillator(80MHz-1GHz).

For the frequency domain applications, from Eq.(2.20), both carrier envelop offset frequency and repetition rate should be stabilized. When the frequency of each line of the comb is stabilized, the whole frequency combs are fixed. When scanning the repetition rate over a frequency interval of the size of the repetition rate, practically all the optical frequencies in the bandwidth of the laser is produced. In this way, the femtosecond laser serves as an optical synthesizer. Also an optical clock can be designed based on the femtosecond frequency comb.[18]

CHAPTER III

CARRIER ENVELOPE PHASE STABILIZATION

Currently there is no direct and easy way to detect the carrier envelope phase, although the effect of the carrier envelope phase can be observed in some experiments[4,5,6]. From Eq.(2.19), it is clear that the carrier and envelope phase shift $\Delta\varphi$ from pulse to pulse, is dependent on the carrier envelope offset frequency and the repetition rate. If one wants to measure the effect of $\Delta\varphi$, it is necessary to detect and stabilize both the carrier envelope offset frequency and the repetition rate. This is achieved with the *f* to 2*f* interferometer.

A. F to 2F Interferometer

1. Self reference technique

One might think to compare the frequency of one of the comb lines to an appropriate very well known atomic or molecular transition to detect the carrier envelop offset frequency. While in principle, this can be done, but such an absolute measurement is not easy and effective. Instead, the self reference is readily applied to detect the carrier envelope offset frequency. The requirement is that the frequency comb spectrum is wide enough to cover an optical octave. In this case the second harmonic generation of the lower frequency end will have the close frequencies with the appropriate comb lines of the higher frequency end. This is depicted in Fig. 8.

The beat signal between the second harmonic comb lines and the fundamental comb lines yield the carrier envelope offset frequency according to

$$2f_n - f_{2n} = 2(nf_r + f_o) - (2nf_r + f_o) = f_o \tag{3.1}$$

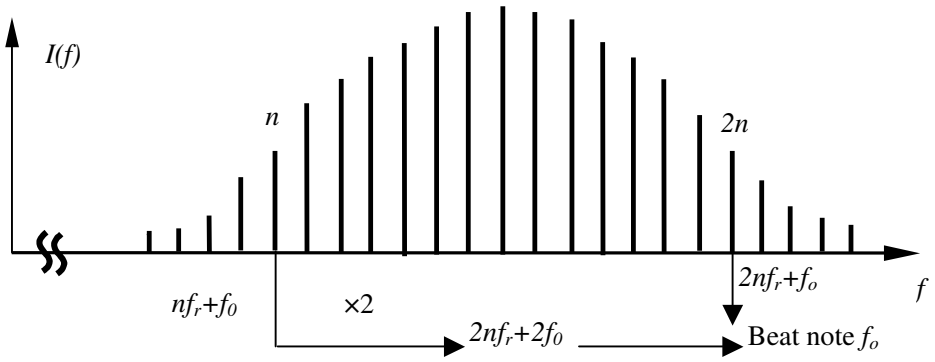

Fig. 8. Self reference

In the nonlinear optics, second harmonic generation actually produces the sum of input frequencies. So the spacing between the comb lines of the second harmonic comb remains f_r. And the portion of the lower frequency end of fundamental comb, which is doubled, is selected by the phase matching in the nonlinear crystal.

The self reference requires an optical octave spectrum. But most femtosecond lasers do not have such a broad octave spectra, and some spectral broadening technique must be used and carried out of the laser cavity.

In the present setup, we use a photonic crystal fiber to achieve an octave spanning spectrum. The fiber has a solid silica core surrounded by air holes. By the strong self phase modulation and Raman scattering, the spectrum is broadened over an optical octave[19,20]. Fig. 9. displays the non-broadened spectrum at the input of the fiber. The broadened spectrum at the output is depicted in Fig. 10. Both spectra were measured with a spectrometer (Oceanoptics USB2000).

The output spectrum is extremely sensitive to the input conditions, such as position, power and the polarization of the laser. If it spans more than one octave, we call it a supercontinuum. Of course the dispersion inside the fiber will change the pulse shape in the time domain, and do it the same way to all the pulses. As a consequence, the pulse

envelope changes, however the periodicity of the pulse envelope remains the same. Thus the spectrum of the pulse trains which come out of the fiber should still has a regular spaced frequency comb[1].

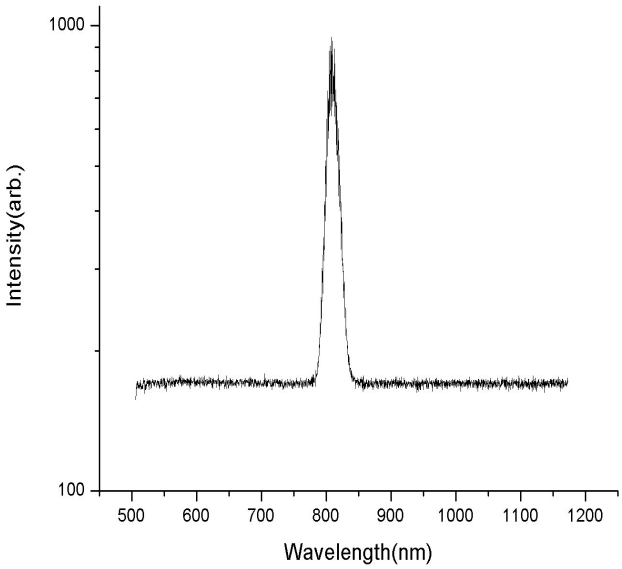

Fig. 9. Spectrum of the initial pulse

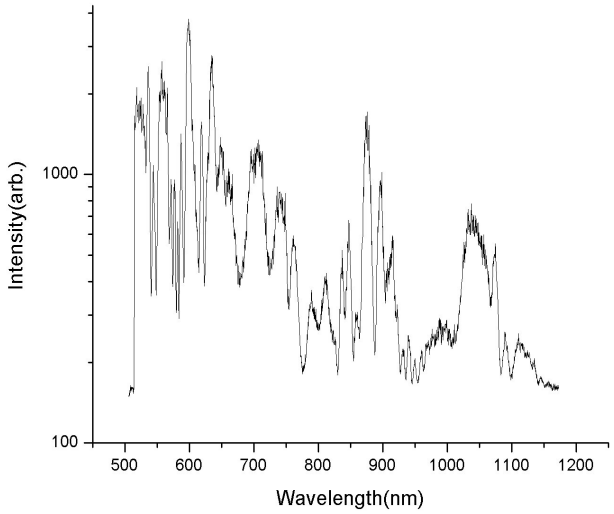

Fig. 10. Spectrum of the output of photonic fiber

2. Optical setup

The optical setup of the *f* to *2f* interferometer is illustrated in Fig. 11.

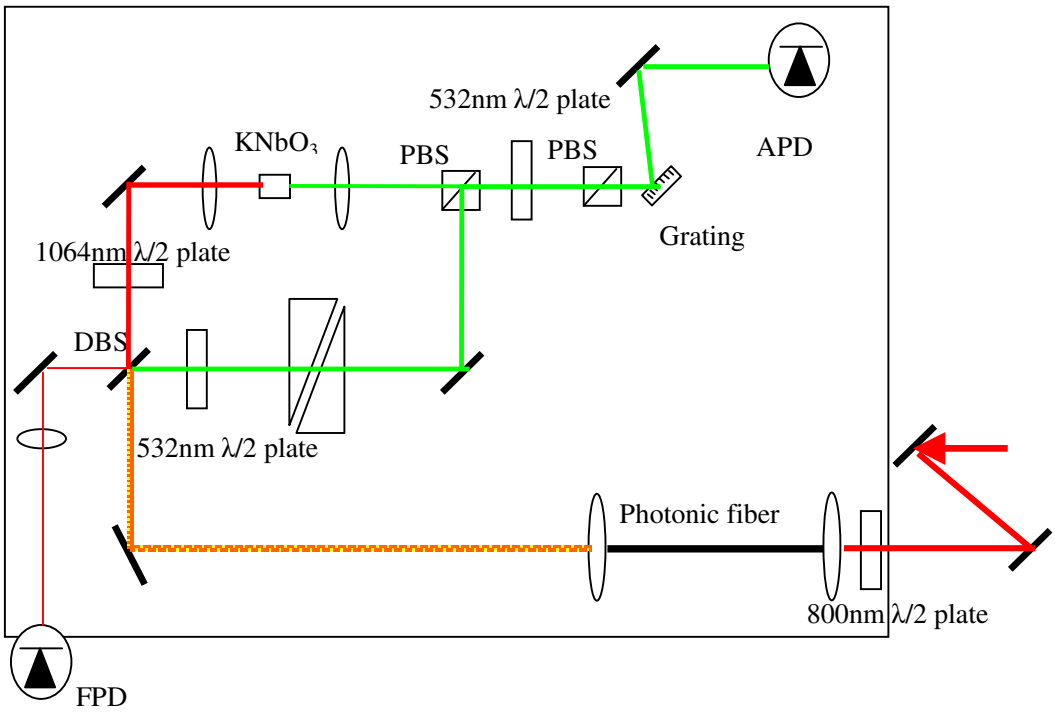

Fig. 11. The *f* to *2f* interferometer

Because the output spectrum of the photonic fiber is extremely sensitive to the input position and the polarization, two mirrors and an 800nm half wave plate are placed before the focusing lens to fine adjust the fiber coupling. Also a very precise lens adjustment is use to optimize the position of the objective to get good coupling of the laser into the fiber. Subsequently an outcoupling objective is used to collimate the output light from the fiber to an appropriate beam diameter. A dichroic beam splitter(DBS) is used to separate the green part of the supercontinuum around 532nm from the infrared part. The green part is reflected along one arm, passes through a 532nm half wave plate

and a pair of glass prism, which serves as a delay line for the temporal overlap. The infrared part is incident along the other arm and passes through the DBS and is frequency doubled in a 5mm long $KNbO_3$ crystal designed for a wavelength around 1064nm. A 1064nm half wave plate is used to adjust the infrared part of the polarization to obtain a strong second harmonic green beam. Because the fundamental and the second harmonic waves have orthogonal polarization, the red part can be removed by a polarization beam splitter(PBS), while the green part from the second harmonic generation will overlap with the green part from the other arm. The fundamental and the second harmonic combs have different polarization, they are mixed with a 532nm half wave plate, projected the polarization onto one axis by another PBS, filtered with a grating to separate other parts and only get the region around the two green parts to the avalanche photo detector(APD, Menlo System S5343).

If all the parts are aligned appropriately, the carrier envelope offset frequency can be observed on a spectrum analyzer(Atten Instruments AT5010) as Fig. 12. The search procedure is outlined in the following section.

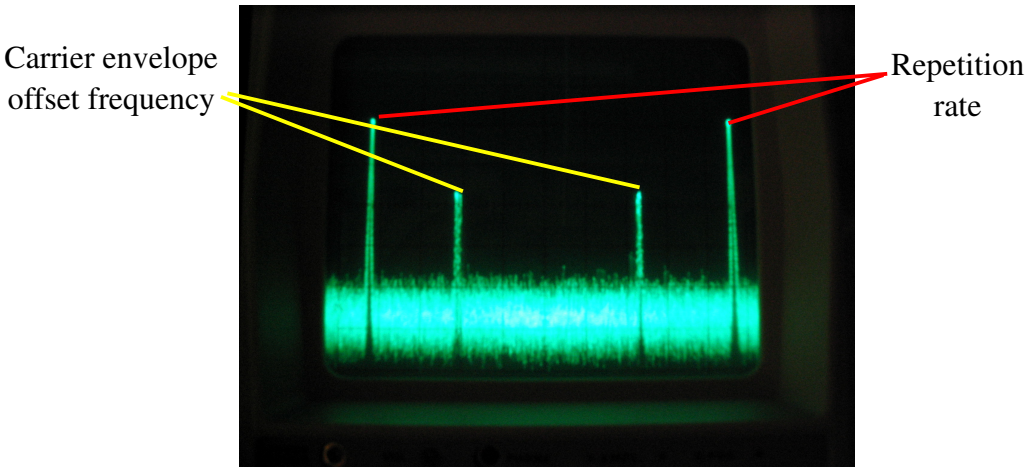

Fig. 12. Carrier envelope offset frequency and repetition rate

B. Alignment Procedure

A proper alignment of *f* to 2*f* interferometer is necessary to get a strong carrier envelope offset frequency. In the following, the adjustment procedure is divided into two parts, the fiber coupling and beat signal searching.

1. Fiber Coupling

Before installing the focusing objective, the two mirrors in front of the interferometer should be used to adjust the laser beam to the entrance of the fiber and as close as possible in the right path to the interferometer, and the working distance of the objective should be checked. The objective should be installed and moved to the proper distance to the fiber. The far field distribution of the focused light should display a good Gaussian beam and kept to the right path in the interferometer.

After the fiber is installed, the objective can be adjusted to get the best fiber coupling namely a maximum of light through. The beam profile after the fiber can be observed with an IR viewer. First, look for large rings on the beam profile, adjust the intensity of rings to make them full of brightness. The central beam profile should look like a Gaussian mode. Then fine adjust the objective and mirrors by walking them off each other to increase the coupling power. For about 200mW input, at least 50mW should be coupled through the fiber. Also a spectrometer could be used to check that the spectrum of the output of the fiber covers an optical octave.

After a good fiber coupling is achieved, the collimating objective should be install. By adjusting the position and the angle, the height of the beam should be around 50mm above the table, and the spot size should be around 1.5mm for the whole path.

2. Beat signal searching

The beat signal is between the second harmonic and fundamental combs. Normally the

second harmonic combs are much weaker than the fundamental combs. To get better signal to noise ratio, it is important to improve the second harmonic combs in the alignment[8]. This is essential to get a good carrier envelope offset frequency signal which can be stabilized.

To get a strong second harmonic generation, first place the filter RG799 in front of the DBS. Adjust the focusing and collimating light into and out of the second harmonic crystal, get a very strong green second harmonic generation. Next, adjust the 1064nm half wave plate behind the DBS, the 800nm half wave plate in front of coupling objective, the two objectives and the two mirrors in front of the coupling objective to get the maximal second harmonic generation. A bright green spot should be seen after the first PBS. Adjust the 532nm half wave plate after the PBS, and the reflecting mirror to make sure the first order diffraction is directed to the entrance to the APD. A bright stripe of green should be seen.

After the strong second harmonic is achieved, the RG799 filter should be removed. The second harmonic comb and fundamental comb should be overlapped at the first PBS by adjusting the DBS, these two spots also should be overlapped at some long distance by adjusting the mirror after the prism pairs. At the entrance to the APD, the two stripes should be overlapped.

After the spatial overlap, the two combs must be overlapped temporally. To achieve this, first approximately estimate the optical paths of the two combs, make them as close to each other as possible with the prism. Then use the prisms as a delay line, slide one prism slowly, look at the spectrum analyzer, which is directly connected with the APD, and search for the beat signal.

Once the beat signal is found, every previous adjustment could be tried to optimize the signal. Sometimes, when sliding the prism, there are two beat signals, both of them could be investigated to see which one could get a better signal to noise ratio.

If no beat signal is found after a thorough search, spatially overlap the two green beams again, and begin another search. A focusing lens in front of APD might be tried to bring more light to the detector and improve the signal to noise ratio. Usually this is not very helpful. In fact, with too much light on the APD, it's easily saturated, which would lower the signal to noise ratio. At least 30dB signal to noise ratio should be obtained. More is better and I have usually 40dB. This is very important for the stabilization of the beat signal, which is just the carrier envelope offset frequency.

C. Electronic Setup

After using the *f* to 2*f* interferometer to detect the carrier envelope offset frequency, we also need some techniques to control and stabilize it. There are two approaches to control it. One is to turn the end mirror in the arm containing the prism pair. Since the spectrum is spatially dispersed on this mirror, a small turn will introduce a linear phase delay with frequency, thus a group delay is produced[8]. The other approach is to change the pump power, so that the pulse power will change with the Kerr lens effect. In this way, we change the carrier envelope phase shift in time domain or the offset frequency in frequency domain[21]. In our laboratory, an acousto-optics modulator(AOM, IntraAction Model ME) is placed in the path of the pump beam to employ the second approach. The zero order beam from the AOM is used to pump the Ti:sapphire femtosecond laser. A voltage control is employed as a feedback of the pump power to adjust the carrier envelope frequency. For stabilization, a phase lock loop was designed to lock the carrier envelope offset frequency to a reference frequency.

1. Phase lock loop

A phase lock loop contains three basic components, a phase detector, a loop filter and a voltage-controlled oscillator (VCO). This is shown as Fig. 13.[22]

The phase detector compares the phase of a reference signal against the phase of the

VCO. The output voltage of the phase detector is proportional to the phase difference between the reference and the VCO. This difference voltage is then filtered by a loop filter and applied to the VCO as the control voltage. The control voltage changes the frequency of the VCO in a direction which will reduce the phase difference between the reference and the VCO. When the loop is locked, the frequency of VCO is exactly same as the reference.

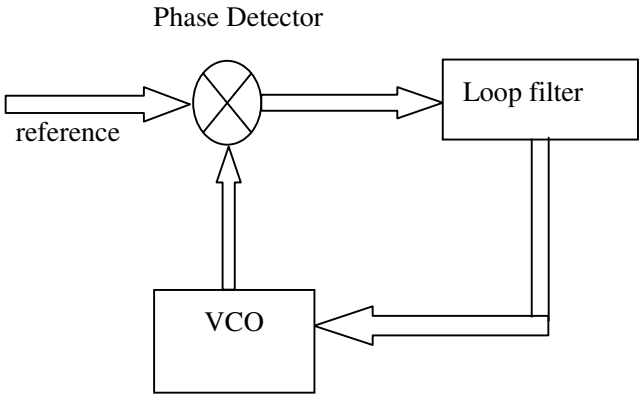

Fig. 13. Basic phase lock loop

The stabilization of the carrier envelope offset frequency is carried out in an analogous way. The actor of the VCO is performed by the femtosecond laser with the AOM. The phase or frequency output of VCO is the carrier envelope offset frequency. The reference signal is a fraction of the repetition rate(for time domain applications) or a reference frequency from a synthesizer(for frequency domain applications). The phase detector is a digital phase detector (MPQ, Garching, Germany), which can track $\pm 16\pi$ phase difference between two sources. The loop filter is a proportional integral controller (MPQ, Garching, Germany). The output of the proportional integral controller is fed to the AOM to stabilize the carrier envelope offset frequency.

2. Electronic setup

The electronic setup for phase stabilization is depicted in Fig. 14.

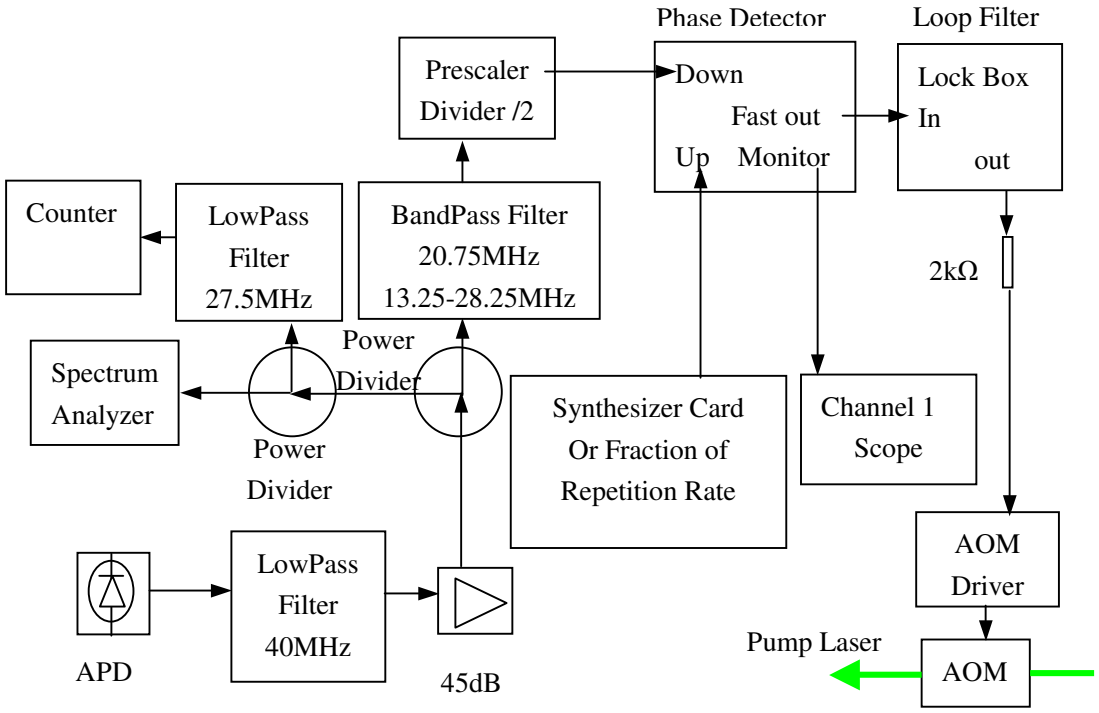

Fig. 14. Electronic setup for the carrier envelope offset frequency stabilization

Basically, the signal received by the APD is filtered by a low pass filter, then amplified and divided to input a spectrum analyzer, an electronic counter and a phase detector separately. The spectrum analyzer and electronic counter are used to monitor and record the carrier envelope offset frequency. Before the phase detector, the signal is divided by 2 by a divider. Thus in the phase detector, half of the carrier envelope frequency is compared with the reference frequency. For frequency domain application, the reference frequency is generated by a synthesizer card. For time domain application, the reference frequency is a fraction of the repetition rate generated by another divider.

Thus, if the output of the synthesizer card is 10MHz, the carrier envelope offset frequency would be stabilized at 20MHz. Or if the repetition rate is 88MHz, and it is divided by 8, the reference frequency is 11MHz, thus the carrier envelope offset frequency would be stabilized at 22MHz. With $\Delta\phi = \frac{\pi}{2}$ from pulse to pulse, that means every fourth pulse looks same.

D. Repetition Rate Stabilization

For frequency domain applications, in addition the repetition rate must be stabilized. Comparatively to the detection of the carrier envelope offset frequency, it is rather easy to detect the repetition rate. Focusing a small portion of the laser pulse or a reflection spot generated in the *f* to 2*f* interferometer to a fast photo diode (FPD, Hamamatsu, Si-PIN S5973), we can readily observe a strong repetition rate signal on the spectrum analyzer or the oscilloscope. In our case, a spot generated by the 1064nm half wave plate reflection is focused on the fast photo diode.

According to Eq.(2.17), the repetition rate depends on the cavity length *L*. To control the repetition rate, a piezo is attached to the output coupler to change the cavity length *L*. Also a similar phase lock loop in Fig. 15. was employed for the stabilization of the repetition rate.

Because the repetition rate is quite strong and stable, the phase detector can be a mixer to detect the frequency difference between the repetition rate and reference frequency provided by a synthesizer (PTS 500). The output of the loop filter is amplified to control the piezo attached to the output coupler. Also an electronic counter(HP 53131A) is used to monitor and record the repetition rate.

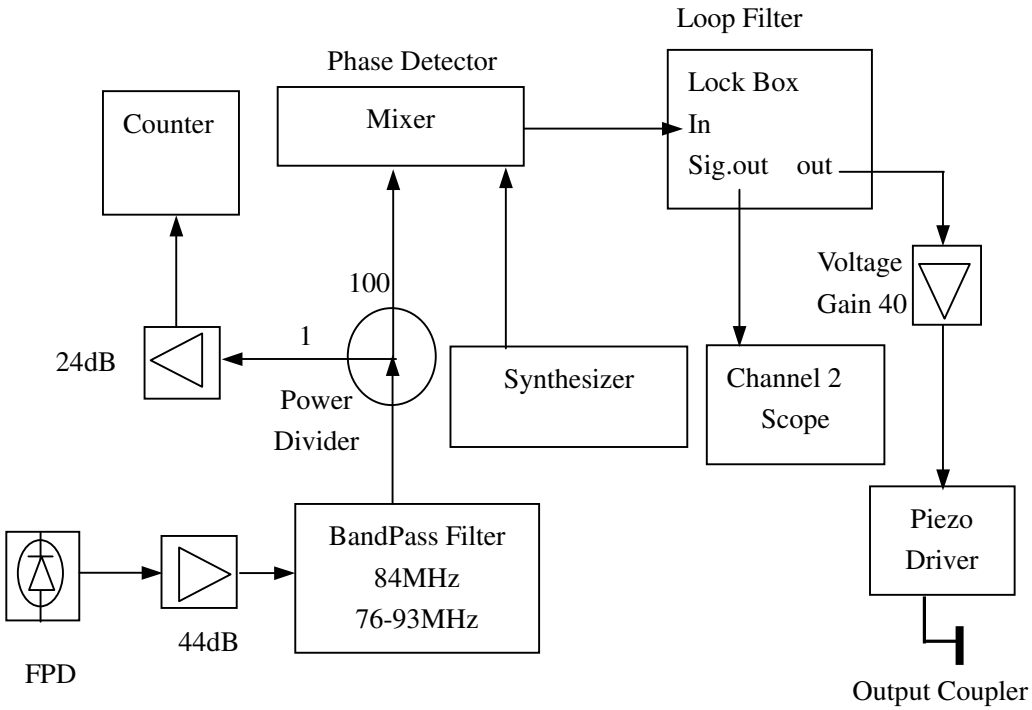

Fig. 15. Electronic setup for the repetition rate stabilization

When both the carrier envelope offset frequency and the repetition rate are locked to two reference frequencies, according to Eq.(2.20), the frequency comb is fixed in the frequency domain. Then many frequency domain applications and in particular our field of interest namely precision spectroscopy can be carried out.

Fig. 16 demonstrates that the carrier envelope offset frequency is locked to near 20MHz(lower counter) and the repetition rate is locked to near 87MHz(upper counter). The locking stability reaches 100mHz for the carrier envelope offset frequency and 10mHz for the repetition rate. And the stability time typically reaches up to an hour.

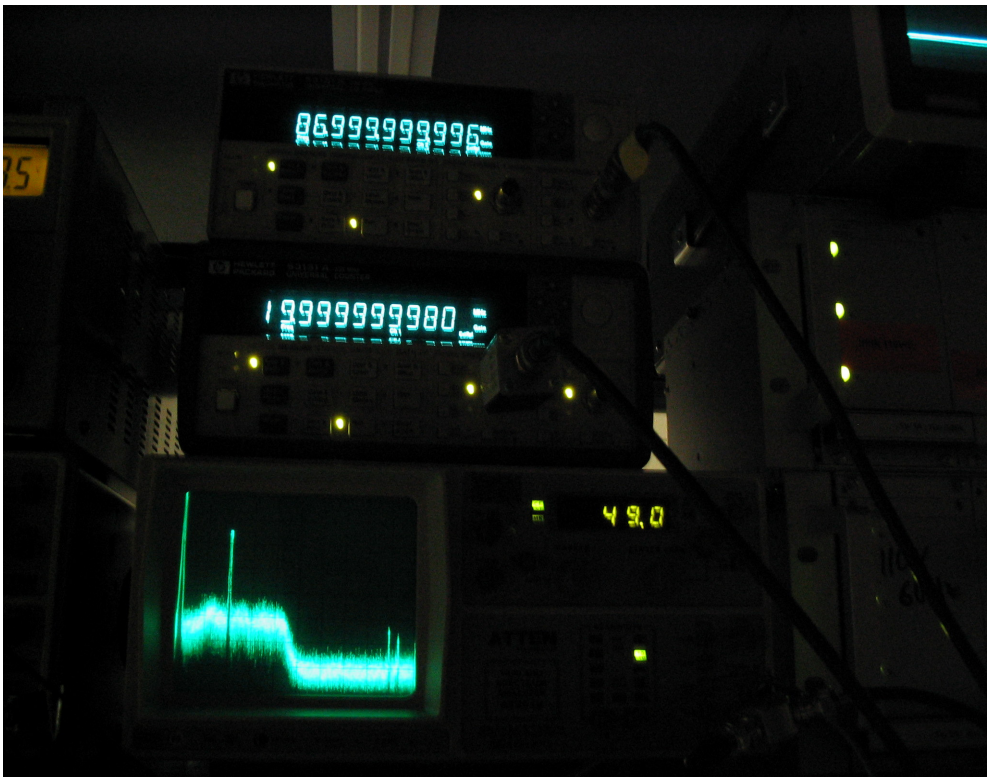

Fig. 16. Stabilization result

Another future project is to improve the timing precision for the whole system. Right now, all the counters, spectrum analyzer, synthesizer are using the 10MHz reference from the PTS synthesizer as the clock. Later on a rubidium frequency standard will be used for the short term stability and a GPS receiver for the long term stability. Then the system will have a precise external clock traceable to National Institute of Standards and Technology (NIST, Boulder Colorado).

CHAPTER IV

DOPPLER FREE IODINE SPECTROSCOPY

Since the development of the Doppler free spectroscopy, the strong and narrow iodine (I_2) absorption lines are widely used for laser stabilization and the optical frequency measurement applications. We have implemented such a saturation spectroscopy setup of the hyperfine spectra of I_2 to provide an accurate frequency reference to lock a CW dye laser. Our first measurement application of frequency comb will measure the frequency of the I_2 stabilized dye laser by beating it with the closed mode in the frequency comb generated by a carrier envelope phase stabilized femtosecond laser.

A. Iodine Absorption Line

The iodine molecule is a diatomic molecule. For diatomic molecules, the wave functions of the energy levels depend on the electron coordinates($\vec{r}$) as well as the nuclear coordinates($\vec{R}_1, \vec{R}_2$). If the Born-Oppenheimer approximation can be used, the total wave function can be separated into a product of the electronic, vibrational, and rotational wave functions[23].

$$\psi(\vec{r}, \vec{R}_1, \vec{R}_2) = \psi_{el}(\vec{r}, R)\psi_{vib}(R)\psi_{rot}(\theta, \varphi) \tag{4.1}$$

Where R is the distance between the two nuclei.

The total excitation energy E of the molecule is the sum of the electronic, vibrational and rotational excitation energy.

$$E = E_{el} + E_{vib} + E_{rot} \tag{4.2}$$

Usually the electronic excitation energy spacing is much larger than the vibrational excitation energy spacing, and vibrational excitation energy spacing is much larger than the rotational excitation energy. This is shown in Fig. 17.

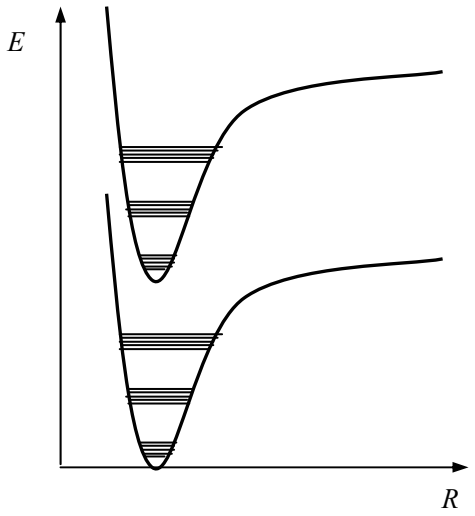

Fig. 17. Vibrational and rotational levels in the electronic states

If a molecule absorbs an photon, it jumps from a lower state to a higher state. The energy difference is the absorption line frequency times Planck's constant. The transition probability between different states can be calculated. Thus the line strength can be obtained[24].

For the iodine molecules, the iodine atoms have large atomic weight, and the chemical bond between the two atoms is weak. Therefore the vibrational frequencies of the molecule are low, and the spacing between the vibrational energy levels is small. Also because of the weak chemical bond, the distance between the two atoms is large, combined with the large atomic weight iodine atoms, the iodine molecule has a large moment of inertia. As a result, the spacing between the rotational energy levels is also small. Thus there are a large number of vibrational and rotational levels in the ground electric state, and a large number of iodine molecules populate these states. As a consequence, there are many iodine absorption lines spanning the main part of the

visible spectrum[25]. Also because of the nuclear electric quadrupole interaction and the magnetic spin interaction, most absorption lines split into the hyperfine structure[26,27]. Together, the iodine molecules have closely spaced absorption lines throughout the visible spectrum. As a consequence, there exits several I_2 absorption line atlases [25,28].

Though the iodine molecules have a great number of absorption lines in the visible spectrum, many of them are not resolved because of Doppler broadening, which is due to the thermal motion of absorbing molecules.

This Doppler broadening is a Gaussian profile with the FWHM[24]:

$$\delta f_D = \frac{f_0}{c}\sqrt{\frac{8kT\ln 2}{m}} \tag{4.3}$$

As an example, putting the mass of iodine molecule into Eq.(3.3), the Doppler broadening at room temperature is about 400MHz at the wavelength of 550nm. While the natural linewidths of hyperfine structure of absorption lines are quite small (around a few MHz magnitude), these hyperfine structures are masked by the Doppler broadening.

B. Doppler Free Absorption Spectroscopy

To observe these hyperfine structures, the technique of laser-saturated absorption is commonly used to avoid the Doppler broadening.

1. Linear and nonlinear absorption

As a simple example, the laser radiation field interacts with two level molecules, the intensity decrease dI of a wave with intensity I propagating along z direction through the absorbing sample is[24]:

$$dI = -I\sigma_{ik}(N_i - \frac{g_i}{g_k}N_k)dz \tag{4.4}$$

Where σ_{ik} is the absorption cross section, which specifies the absorption per molecule, N_i and N_k are the population densities of the lower level E_i and higher level E_k,

g_i and g_k are the degeneracy coefficients of E_i and E_k.

When a weak radiation field interacts with molecules, the change of level populations can be neglected, and the absorbed intensity is proportional to the incident intensity. This is linear absorption with

$$I(z) = I_0 \exp(-\alpha z) \tag{4.5}$$

with $\alpha = \sigma_{ij}[N_i - \frac{g_i}{g_k} N_k]$ being the absorption coefficient

When a strong radiation field interact with molecules, the population density N_i of lower state E_i will significantly decrease, while the upper density N_k increases. Therefore dI is no longer proportional to I. This is nonlinear absorption.

When $N_i = \frac{g_i}{g_k} N_k$ is reached, the absorption coefficient goes to zero, the sample becomes completely transparent, so that no more photons can be absorbed by the sample. This effect is called saturation of the absorption.

2. Doppler free saturation spectroscopy

The saturation of absorption can be used to target the group of molecules, which are not moving in the direction of laser beam. Thus, the spectroscopy does not show the Doppler broadening. To achieve this, two beams with the same frequency f_0 are sent through an iodine vapor absorption cell. These two beams are overlapped in the iodine cell and traveled in the opposite direction. One of the beams is much stronger than the other, it is called the pump beam. And the other beam is called the probe beam. The pump beam is periodically chopped, the intensity of the probe beam, which is modulated because of saturation of the absorption, is detected by photon detectors. Assume the pump beam is traveling in the z direction, then the probe beam travels in the $-z$ direction. Because of the Doppler shift, the molecules with a velocity $\vec{v}$ see the frequency of the pump beam

as $f_0(1-v_z/c)$ and the frequency of the probe beam as $f_0(1+v_z/c)$. Thus only the molecules with $v_z=0$ can see the both beams with the same frequency f_0. If f_0 is tuned close to one of the absorption frequencies of the molecules, the transmission of the probe beam will be enhanced due to the saturation of the absorption of those molecules with $v_z=0$.

C. Doppler Free Saturation Iodine Spectroscopy

The iodine molecules have many possible transitions with slightly different frequencies. If these transitions are independent, the observed saturation spectroscopy is the superposition of these different transitions.

It is possible to achieve the transmission increase of the probe beam by the saturation effect. And many techniques are usually used to increase the signal to noise ratio. The set up for the Doppler free saturation iodine spectroscopy which was used in this experiment is shown as Fig. 18.

In additional to the probe beam is overlapped with the pump beam, another probe beam parallel with the overlapped probe beam is directed through the 25cm iodine cell. This probe beam is not overlapped with the pump beam, so there is no effect of saturation on it. The two probe beams have similar power, and the difference of the transmission of the two beams is detected by a differential photodetector. To improve the overlap of the pump beam and one of the probe beam, a 550nm half wave plate and a polarizing beam splitter cube is used to fully overlap the pump and probe beam, though the polarization of these two beams are different, the saturation effect still remains. To improve the signal to noise ratio, a chopper is placed in the path of pump beam. The chopper periodically blocks the pump beam, thus the saturation effect of the overlapped probe beam is periodically removed and introduced, therefore the amplitude of the transmission of this probe beam is modulated by the chopper, this modulation can be detected by a lock-in amplifier. The use of the signal modulation and lock-in amplifier

significantly increases the signal to noise ratio.

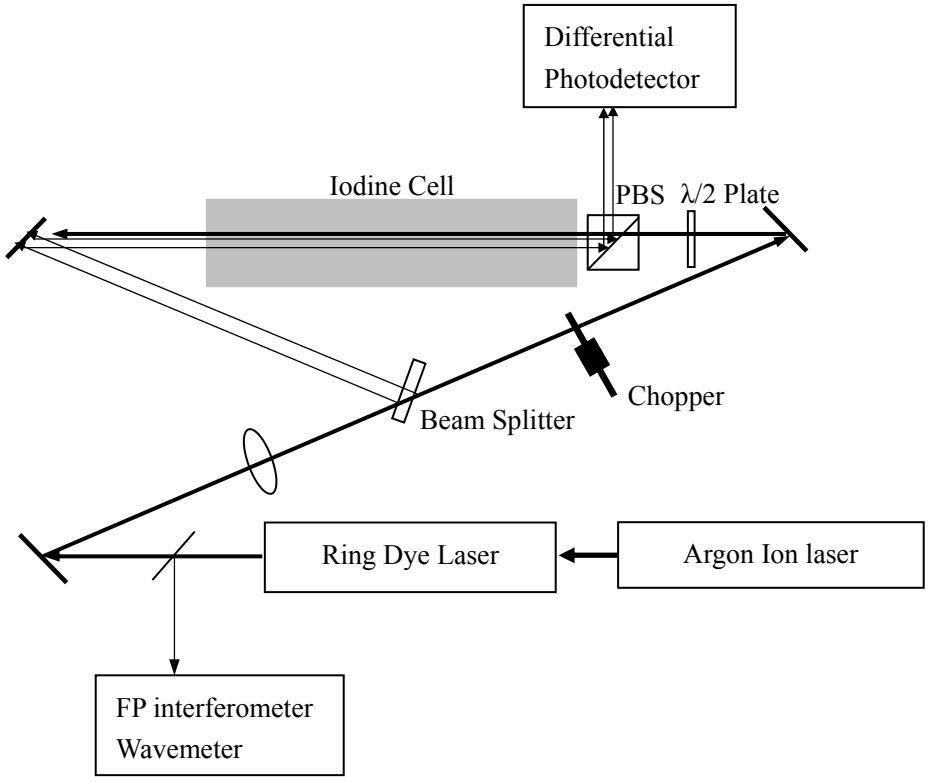

Fig. 18 Optical setup of the Doppler free iodine spectroscopy

1. Optical setup

The performance of the CW tunable ring dye laser pump is critical to the experiments. The ring dye laser(Coherent, 699-21) is pumped by an argon ion laser(Coherent, Innova series). Lambdachrome dye Rhodamine 110(R110) dissovled in ethylene glycol is used as the gain medium. The ring dye laser can be operated stably at a single mode. The manufacturer specified linewidth is 1MHz, due to the laser jet fluctuations and acoustic noise the output frequency fluctuates and the effective linewidth is about 3MHz, which is derived by the Coherent manual. When operated properly, the tuning range of the ring

dye laser with R110 is from 530nm to 580nm with the peak at about 550nm. And it can scan 30GHz without mode hopping.

Also to monitor the single mode structure, a scanning F-P interferometer is used. In this way, any malfunction or mode hopping of the ring dye laser can be detected. To measure the laser frequency, a wavemeter (Burleigh, WA-10) is used. The resolution of the wavemeter is $0.01cm^{-1}$, corresponding to about 300MHz.

For the Doppler free iodine spectroscopy, only a small portion from the output of the ring dye laser is used. The power of the pump beam is around 9mW, and the power of each probe beam is around 0.3mW. A lens with focal length 50cm is employed to increase the intensity of these beams to improve the saturation effect of the probe beam overlapped with the pump beam.

2. Electronic setup

The electronic setup is depicted in Fig. 19.

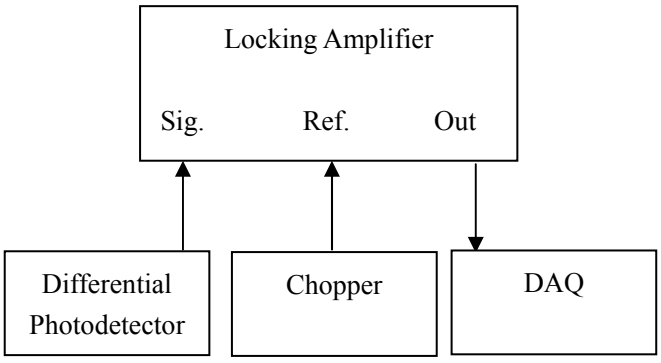

Fig. 19. Electronic setup of Doppler free iodine spectroscopy

The chopper modulated transmission difference between the two probe beams is detected by a differential photodetector. It is sent to the signal channel of the lock-in

amplifier (EG&G, Model 124A). The synchronization signal from the chopper (EG&G, Model 198) is sent to the reference channel of the lock-in amplifier. The output of the lock-in amplifier is sent to a DAQ device (NI, M6221) to collect the data. If necessary, the timing of a scan can also be controlled by the DAQ output to the laser control box.

3. Spectroscopy and comparison

The tuning range of the ring dye laser is dependent on argon ion laser pump power and the age of the dye. The useful lifetime of R110 is only about 50W·h. When it is operated around 545nm, the whole systems perform well. And the iodine absorption spectroscopy for this region is shown in Fig. 20., Fig. 21. and Fig. 22. for different scan widths.

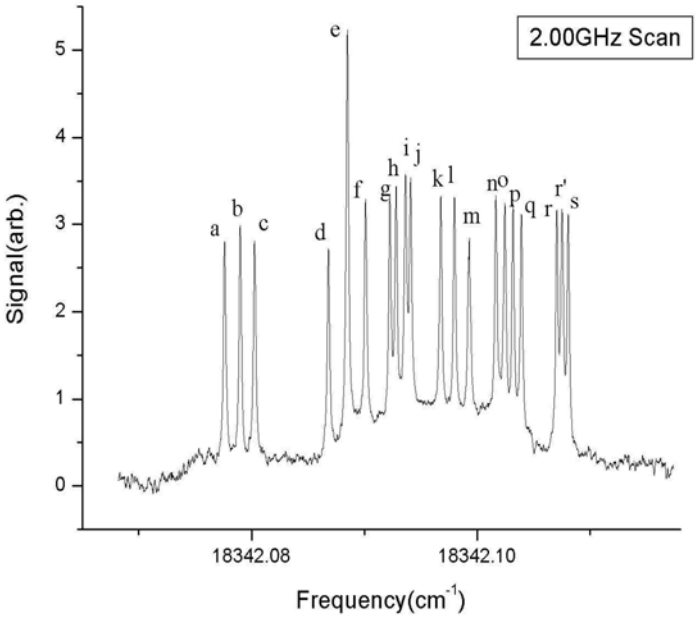

Fig. 20. Iodine saturation signal(2.00GHz scan)

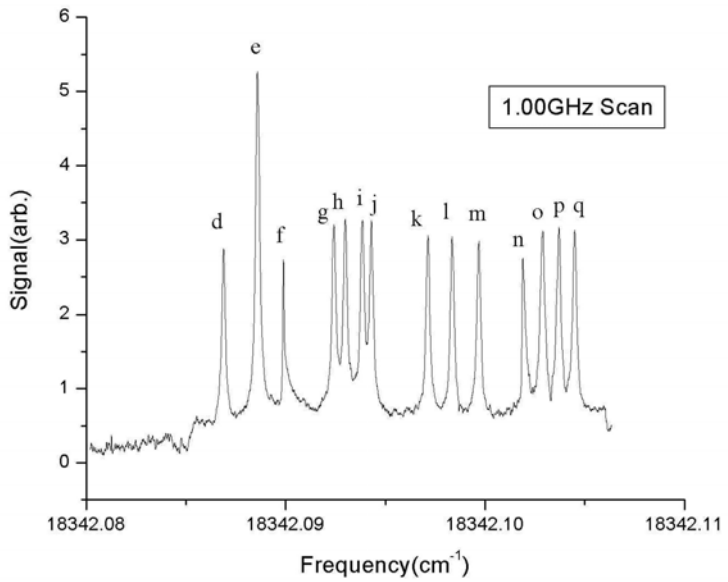

Fig. 21. Iodine saturation signal(1.00GHz scan)

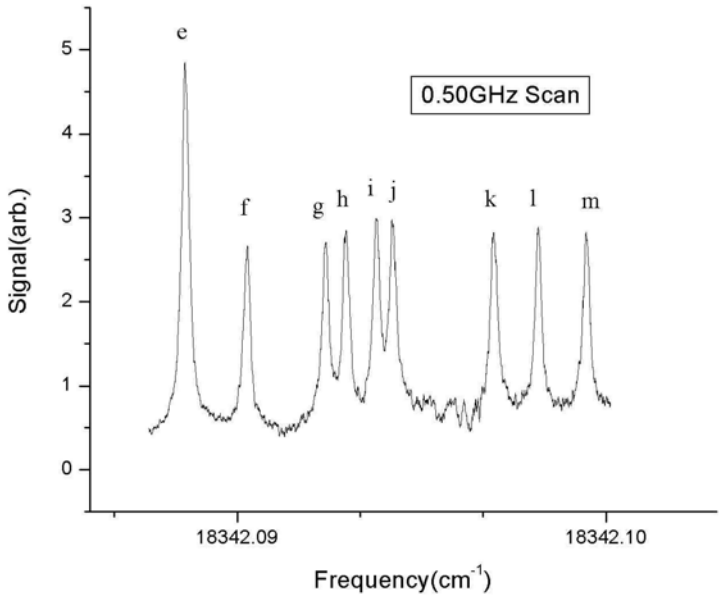

Fig. 22. Iodine saturation signal(0.50GHz scan)

The different scan widths repeat the iodine absorption line quite well. As can be seen from the Fig. 22., there are several narrow spectral lines. Each of these lines can be used for frequency locking of the dye laser. Most of these strong and narrow absorption lines are listed in the I_2 atlas, which serves as a good reference.

Using the iodine line atlas[28], the frequencies of the absorption lines are calculated. The data in the atlas does not show the splitting for the line *r*, which our setup could resolve. The splitting of line *r* is around 6MHz. The frequencies of the absorption lines are summarized in Table I.

Table I. Iodine hyperfine line frequency data

Line	Frequency, cm^{-1}
a	18342.07871
b	18342.07977
c	18342.08076
d	18342.08778
e	18342.08917
f	18342.09063
g	18342.09315
h	18342.09355
i	18342.09421
j	18342.09454
k	18342.09765
l	18342.09871
m	18342.09991

Table I. continued

Line	Frequency, cm^{-1}
n	18342.10229
o	18342.10309
p	18342.10368
q	18342.10434
r	18342.10805
s	18342.10845

CHAPTER V

SCHEME FOR THE DIRECT MEASUREMENT OF AN OPTICAL FREQUENCY

In the frequency domain, one of the applications of the carrier envelope phase stabilized pulse is to directly measure the optical frequency. In this chapter, the basic principle and the set up of experiment and problems are discussed.

A. Basic Pringciple

As Eq.(2.20), if the repetition rate and the carrier envelope offset frequency is locked to reference frequencies, the whole frequency comb is fixed. If the beat signal between the one line of the frequency comb and a single frequency CW laser can be detected, the optical frequency of the CW laser should be

$$f_{cw} = f_o + nf_r \pm f_{beat} \tag{5.1}$$

To exactly determine the optical frequency of the CW laser, the integer n and the ± need to be solved. Suppose the CW laser is tunable, the frequency f_{cw} can be slightly changed to one direction, if the f_{beat} move with the same direction, it would be plus sign, otherwise, it would be minus sign. To determine the large integer n, if the resolution of a good wavemeter is smaller than the repetition rate, the frequency of the CW laser can be coarsely measured by the wavemeter. Thus the n can be determined easily. Or the iodine saturation spectroscopy could provide a good reference[29]. Another trick is to change the repetition rate[30,31]. All these techniques could be used to determine the optical frequency of the CW laser.

B. Detection Method

In order to measure the frequency of the CW laser, the beat signal between one mode of

the frequency comb and CW laser must be detected despite a large number of other modes of the comb as noise. To prevent the noise from reaching the photodetector, a grating can be used to spatially filter out a lot of other modes. And the signal to noise ratio of the beat signal between the CW laser and *n*th mode on a photodetector with quantum efficient η and detecting bandwidth B_w can be calculated from[32]:

$$\frac{S}{N} = \frac{\eta}{h\nu B_w} \frac{tP_n(1-t)P_{CW}}{t\sum_k P_k + (1-t)P_{CW}} \tag{5.2}$$

Where $h\nu$ is the single photon energy, P_{CW} is the power of the CW laser, P_n is the power of the *n*th mode of frequency comb, t is the effective transmission coefficient of the adjustable beam splitter used to overlap the CW laser and frequency comb. The summation of k is the modes of comb, which reach the photodetector.

To simplify the equation, assume $P_k=P_n$ that every mode has the same power and there are M modes of the frequency comb reach the photodetector, thus

$$\frac{S}{N} = \frac{\eta}{h\nu B_w} \frac{tP_n(1-t)P_{CW}}{tMP_n + (1-t)P_{CW}} \tag{5.3}$$

Also assuming the t is adjusted to get the optimum signal to noise ratio,

$$t_{opt} = \frac{\sqrt{P_{CW}}}{\sqrt{P_{CW}} + \sqrt{MP_n}} \tag{5.4}$$

And usually with the spatial filtering of the grating, the power of the CW laser is much larger than power of all the frequency comb modes reaching the photo detector $P_{CW}>>MP_n$, thus the optimum signal to noise ratio is

$$\frac{S}{N}_{opt} = \frac{\eta P_n}{h\nu B_w} \tag{5.5}$$

Thus to improve the signal to noise ratio, it is important to maintain the weak signal as much as possible.

C Experimental Setup

The experiment setup is depicted in Fig. 23.

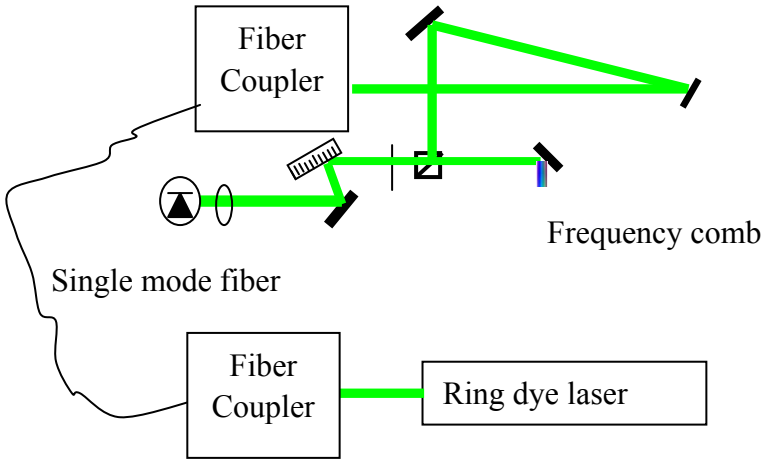

Fig. 23. Experimental setup for optical frequency measurement

Because of the space limitation, a single mode fiber is used to guide the CW laser from a ring dye laser(Coherent, 699-21) at the other table to the optical table where the frequency comb is produce and the beat signal detector is located. The single mode fiber coupling is around 20%. The CW laser out of the fiber overlap with a frequency comb beam from the *f* to *2f* interferometer at a non-polarization beam splitter. They pass through a polarization film, and are diffracted by a grating. The first order diffraction of grating is focused by a 1.5cm lens placed 50cm away from the reflect mirror. A photo diode(Hamamastu, Si-PIN S5973) is used to detect the signal.

The beam from the two PBS of *f* to *2f* interferometer contains the frequency mode close to the dye laser, thus they can be used for the optical frequency measurement. A spectrum analyzer directly connects the output of the photo diode to display the signal. So far, I have not yet foundd the beat signal between the frequency comb and CW dye

laser. Typically I see on the spectrum analyzer is a strong repetition rate signal from the frequency comb and several weak lines around 0~40MHz from the dye laser.

To find the beat signal between the CW dye laser and one mode of frequency comb, several improvements need to be made.

The beam splitter cube is a non polarization beam splitter, transmission and reflection is around 50% each, thus almost half of the comb power is lost. As Eq.(5.5), the weak signal need to be maintained as much as possible. Thus using a polarization beam splitter with two half wave plates to change the polarization of the comb and dye laser wild be a better choice.

The polarizer is a polarizing film, which has a lot of losses. It is arranged the same as the polarization direction with comb. It would be better to use a polarization beam splitter with a half wave plate to find the best transmission of the dye laser and comb.

For the grating, the major power diffracted does not go to the first order. When tested with dye laser, only about 25% first order efficiency at the 60° blazing angle. It needs to be changed to another one with higher first order efficiency.

Also the adjustments of ring dye laser and femtosecond laser are critical to the experiment. Only when both lasers work properly, can we achieve good experimental result.

We are presently taking care of these improvements and expect to find the beat signal in the near future.

CHAPTER VI

SUMMARY AND CONCLUSIONS

The carrier envelope phase of our femtosecond laser was stabilized and ready for the frequency domain applications. These are the direct optical frequency measurement in progress, and later on precision spectroscopy.

Because the performance of the Ti:sapphire laser is critical to the carrier-envelope phase stabilization, a linear and folded laser resonator was discussed to provide a guideline for the femtosecond laser adjustment. The shot pulse trains emitted by the femtosecond laser were also discussed analytically to provide a theoretical basis for the carrier envelope phase stabilization.

An *f* to *2f* interferometer described and was used to detect the carrier envelope offset frequency, and a fast photo diode was used to detect the repetition rate. Similarly designed phase locked loops were used to stabilize the carrier envelope offset frequency and the repetition rate to the reference frequencies. The stability reaches 100mHz for the carrier envelope offset frequency and 10mHz for the repetition rate up to an hour. This is prerequisite for the future frequency domain applications.

Saturation spectroscopy has been implemented and the hyperfine spectra of the iodine molecule in the R110 region were obtained. It can provide an accurate frequency reference. One of these narrow, strong and stable iodine absorption lines is being used to lock the laser.

The scheme to measure the optical frequency is described. The problems in the experiments are discussed. With improvement on the instruments, better result will be achieved.

For the future precision spectroscopy of iodine molecule, first we need to lock the ring dye laser on one of the selected iodine absorption line. This can be realized by the

frequency modulation introduced by an acousto-optic modulator. The dispersion like error signal generated by the frequency modulation can be used to lock the dye laser on one of the selected iodine absorption line. Then we need find the beat signal between the one mode of femtosecond frequency comb and the dye laser. Once the beat signal is found, with some electronic improvement, the precision spectroscopy of iodine will be achieved.

REFERENCES

[1] Th. Udem, R. Holzwarth, and T.W. Hänsch, Nature **416**, 233 (2002)

[2] S.T. Cundiff, J.Phys.D **35**, R43 (2002*)*

[3] T. Brabec and F. Krausz, Rev. Mod. Phys. **72**, 545 (2000)

[4] G.G. Paulus, F. Grabon, H. Walther, P.Villoresi, M. Nisoli, S. Stagira, E. Priori, and S. De Silvestri, Nature **414**, 182 (2001)

[5] C.G. Durfee, A.R. Rundquist, S. Backus, C. Herne, M.M. Murnane, and H. C. Kapteyn, Phys.Rev. Lett. **83**, 2187 (1999)

[6] A. Batusika, Th. Udem, M. Uiberacker, M. Hentschel, E. Goulielmakis, Gh. Gohle, R.Holzwarth, V.S. Yakovlev, A. Scrinzi, T.W. Hänsch, and F. Krausz, Nature **421**, 611 (2003)

[7] Th. Udem, J. Reichert, R. Holzwarth, and T.W. Hänsch, Phys.Rev.Lett. **82**, 3568 (1999)

[8] J. Reichert, R. Holzwarth, Th. Udem, and T.W. Hänsch, Opt. Comm. **172**, 59 (1999)

[9] M. Takamoto, F. Hong, R. Higashi, and H. Katori**,** Nature **435**, 321 (2005)

[10] D.E.Spence, P.N. Kean, and W.Sibbett, Opt.Lett. **16**, 42 (1991)

[11] M.Piche, Opt. Commun. **86**, 156 (1991)

[12] A.E. Siegman, *Lasers* (University Science Books, Mill Valley, California, 1986)

[13] H.W. Kogelnik, E.P. Ippen, A. Dienes, and C.V. Shank, IEEE J. of Quan. Elec. **8**, 373 (1972)

[14] J. Turunen, Appl. Opt. **25**, 2908 (1986)

[15] H. Kogelnik and T. Li, Appl. Opt. **5**, 1550 (1966)

[16] T. Brabec, P.F. Curley, Ch. Spielmann, E.Winter, and A.J. Schmidt, J. Opt. Soc. Am.B **10**, 1029 (1993)

[17] C. Spielmann, P.F. Curley, T. Brabec, and F. Krausz, IEEE J. of Quan. Elec. **30**, 1100 (1994)

[18] Th. Udem, Nature **435**, 291 (2005)

[19] J.K. Ranka, R.S. Windeler, and A.J. Stentz, Opt. Lett. **25**, 25 (2000)

[20] J.K. Ranka, R.S. Windeler, and A.J. Stentz, Opt. Lett. **25**, 796 (2000)

[21] H.A.Haus and E.P. Ippen, Opt. Lett. **26**, 1654 (2001)

[22] F. M. Gardner, *Phaselock Techniques* (John Wiley&Sons, New York, 1979)

[23] H. Haken and H.C.Wolf, *Molecular Physics and Elements of Quantum Chemistry* (Springer, New York, 2004)

[24] W. Demtroder, *Laser Spectroscopy* (Springer, New York, 1981)

[25] S. Gerstenkorn and P.Luc, *Atlas du Spectre d'Absorption de la Molecule d'Iode*

14800-20000 cm^{-1} (Editions du Centre National de la Recherche Scientifique, Paris, 1978)

[26] M. Levenson and A. Schawlow, Phys. Rev. A **6**, 10 (1972)

[27] T.W. Hänsch, M.D. Levenson, and A.L. Schawlow, Phys. Rev. Let. **26**, 946 (1971)

[28] H. Kato, M. Baba, S. Kasahara, K. Ishikawa, M. Misono, et al., *Doppler-Free High Resolution Spectral Atlas of Iodine Molecule 15,000 to 19,000 cm^{-1}*(Japan Society for the Promotion of Science, Japan, 2000)

[29] A.Y.Nevsky, R. Holzwarth, J.Reichert, Th. Udem, T.W. Hänsch, J.Von Zanthier, H. Walther, H.Schnatz, F.Riehle, P.V. Pokasov, M.N. Skvortsov, and S.N. Bagayev, Opt. Comm. **192**, 263 (2001)

[30] R.Holzwarth, A.Y. Nevsky, M. Zimmermann, Th. Udem, T.W. Hänsch, J.Von Zanthier, H. Walther, J.C. Knight, W.J. Wadsworth, P.ST.J. Russell, M.N. Skvortsov, and S.N. Bagayev, Appl.Phys.B **73**, 269 (2001)

[31] S.T. Cundiff and J. Ye, Rev. Mod. Phys. **75**, 325 (2003)

[32] R.H.Kingston, *Detection of Optical and Infrared Radiation* (Springer, New York, 1978)

VITA

Feng Zhu was born in the People's Republic of China. He received his B.S. degree in 1998 from the Department of Physics, Tsinghua University, Beijing, P.R.China. He received his M.S. degree in 2001 from the Department of Physics, Tsinghua University, Beijing, P.R.China. He was admitted to the graduate school of Texas A&M University in 2002, and received his M.S. in physics in 2005. For his address and other current information, please contact Dr. Hans Schuessler, Department of Physics, Texas A&M University, College Station, TX 77843-4242.